# Intermittency of three-dimensional perturbations in a point-vortex model

Adrian van Kan,* Alexandros Alexakis,† and Marc-Etienne Brachet‡
*Laboratoire de Physique de l'Ecole normale supérieure, ENS, Université PSL, CNRS, Sorbonne Université, Université de Paris, F-75005 Paris, France*
(Dated: January 12, 2021)

Three-dimensional (3-D) instabilities on a (potentially turbulent) two-dimensional (2-D) flow are still incompletely understood, despite recent progress. Here we propose a simple energy-conserving model of a regularised 2-D point-vortex flow coupled to localised 3-D perturbations ("*ergophages*"), such that *ergophages* can gain energy by altering vortex-vortex distances through an induced divergent velocity field, thus decreasing point vortex energy. We investigate the model in three distinct stages of evolution: (i) The *linear regime*, where the amplitude of the *ergophages* grows or decays exponentially on average, with an instantaneous growth rate that fluctuates randomly in time. The instantaneous growth rate has a small auto-correlation time, and a probability distribution featuring a power-law tail with exponent between $-2$ and $-5/3$ (up to a cut-off) depending on the background state of the point-vortex flow. Consequently, the logarithm of the *ergophage* amplitude performs a free Lévy flight. (ii) The *passive-nonlinear* regime of the model, where the 2-D flow evolves independently of the *ergophage* amplitudes, which saturate by non-linear self-interactions without affecting the 2-D flow. In this regime the system exhibits a new type of on-off intermittency that we name *Lévy on-off intermittency*, which we define and study in a companion paper [1]. We compute the bifurcation diagram for the mean and variance of the perturbation amplitude, as well as the probability density of the perturbation amplitude. (iii) Finally, we characterise the the *fully nonlinear regime*, where *ergophages* feed back on the 2-D flow, and study how the vortex temperature is altered by the interaction with ergophages. It is shown that when the amplitude of the *ergophages* is sufficiently large, the 2-D flow saturates to a zero-temperature state. Given the limitations of existing theories, our model provides a new perspective on 3-D instabilities growing on 2-D flows, which will be useful in analysing and understanding the much more complex results of DNS and potentially guide further theoretical developments.

## I. INTRODUCTION

Point vortex flow is a simple (but singular) exact solution of the two-dimensional (2-D) Euler equation describing inviscid fluid flow, in which $N$ strongly localised vortices advect each another chaotically by their induced velocity fields [2–4]. They admit a famous equilibrium statistical mechanics description due to Onsager [5, 6], who showed that states with negative temperatures exist in the system, where same-signed point vortices cluster to form two strong counter-rotating vortices. Indeed, 2-D turbulent flow features isolated vortices which aggregate and merge over time in a process called *inverse energy cascade* to form a large-scale *condensate*, where most of the energy is concentrated in the largest-scale mode [7–9]. This is in contrast with three-dimensional (3-D) turbulence, where energy is transferred from large to small scales [10]. Inverse cascades and associated condensation phenomena are also found in quasi-2-D flows, such as turbulence in thin layers [11–15] and rapidly rotating turbulence [16, 17], which feature 3-D components, but are predominantly 2-D. A review of such flows is given in [18].

Point vortex models have found numerous applications in simplified descriptions of turbulent fluid flows. An early successful simulation of the inverse cascade in 2-D turbulence indeed relied on the point-vortex-based vortex-in-cell approximation, [19]. In the 1990s, there was a significant activity devoted to vortex gas modelling of (particularly decaying) 2-D turbulence [20–24], where merging rules for point vortices were prescribed, yielding 2-D turbulence-like behavior at reduced numerical cost. Point vortex models have also been used to investigate stirring by chaotic advection [25], as well as Lagrangian intermittency, pair dispersion and transport in turbulence [26–28]. Recently, vortex gas scaling arguments were leveraged to find a highly accurate local closure in baroclinic turbulence [29]. Other physical problems which have been fruitfully treated by point vortex models include the stability of vortex streets and vortex sheets [30–33], quantum turbulence [34–37], plasma dynamics [38] and stellar dynamics [39].

For flows in thin layers, rotating flows and flows under the action of an external magnetic field, it has been proven using upper bound theory [40, 41] that a non-dimensional threshold exists in terms of the layer depth and fluid viscosity (as well as the rotation rate and or the external magnetic field, if present), where the flow undergoes exact bi-dimensionalisation (for periodic or stress-free boundary conditions). Beyond this point, 3-D perturbations away from a 2-D flow decay due to the action of viscous damping. This has profound consequences for turbulent flows since, as mentioned, the phenomenology of 2-D turbulence differs strongly from the 3-D case due to additional conserved quantities in the

* avankan@ens.fr
† alexakis@phys.ens.fr
‡ marc.brachet@gmail.com

2-D case [9, 10]. Therefore, it is important to understand quasi-two-dimensional flows close to the onset of three-dimensionality. The bounding theory only establishes the existence of a threshold, but since it is built on rather conservative estimates, it cannot capture the physics occurring near the threshold. Very recently, in an extensive numerical study [42], Seshasayanan and Gallet investigated the linear stability of 3-D perturbations on a 2-D turbulent condensate background flow at the onset of three-dimensionality. The authors showed that when instability is present, the time evolution of the energy of linear 3-D modes involves phases of jump-like exponential growth occurring randomly in time, inter-spaced by plateau-like phases where growth is absent. Here, in the spirit of the wide range of applications of point vortices described above, we present and analyse a point vortex model of localised 3-D perturbations in quasi-2-D turbulence, whose dynamics are qualitatively similar to the exponential growth and decay evolution found in [42].

The remainder of this article is structured as follows. In section II, we provide a brief introduction to the concept of point vortex temperature, in section III, we formulate the model to be studied. In section IV, we describe the method of our investigation. Then, in section V we present the results of our numerical simulations and finally in section VI we discuss the implications of our results and remaining open questions.

## II. BACKGROUND: TEMPERATURE OF POINT VORTEX STATES

We briefly summarise the concept of the temperature of point vortex flow, which was introduced in 1949 by Onsager [5]. The energy of a set of point vortices is given by the Hamiltonian $H$, which only depends on the vortex positions $(x, y)$. These positions are the conjugate variables of the point vortex Hamiltonian. In bounded domains, the total phase space volume is therefore finite. We denote by $\Omega(E)$ the phase space volume occupied by states whose energies $H$ lie in the interval $[E, E + dE]$. Then the thermodynamic entropy is $k_B \ln(\Omega(E)/\Omega_0)$, where $k_B$ is the Boltzmann constant and $\Omega_0$ is a reference volume required for dimensional reasons. In the extreme situation where vortex dipoles (vortex-antivortex pairs) collapse, which corresponds to negative energies $E < 0$, the available phase space volume is vanishingly small, $\Omega(E) \overset{E\to-\infty}{\longrightarrow} 0$. The opposite limit of large positive energies occurs when like-sign vortices concentrate at a point, in which case also $\Omega(E) \overset{E\to\infty}{\longrightarrow} 0$. Since the total volume is non-zero, the non-negative function $\Omega(E)$ must reach a maximum at an intermediate energy $-\infty < E_m < \infty$. The associated microcanonical inverse temperature,

$$\beta(E) \equiv \frac{\partial \ln(\Omega(E))}{\partial E} \tag{1}$$

is thus positive for $E < E_m$, but vanishes at $E = E_m$ and is negative for $E > E_m$. Negative-temperature states

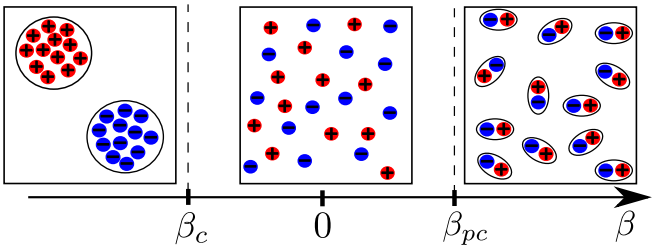


FIG. 1. Overview of point vortex states at negative, zero and positive inverse temperatures $\beta$. Clustering occurs for $\beta < \beta_c < 0$, a homogeneous state is found at $\beta = 0$, and pair condensation occurs for $\beta > \beta_{pc}$.

can generally arise in both classical and quantum systems with a finite number of degrees of freedom whose state space is bounded, such as localized spin systems [43–45]. In the point vortex system, high-energy states at negative temperatures, corresponding to condensates featuring same-sign vortex clusters, have been extensively studied since Onsager's initial contribution [5, 6, 46]. In particular, there is a negative clustering temperature $\beta_c$, which marks the onset of same-sign vortex clustering. Similarly, there is a positive pair condensation temperature $\beta_{pc}$, at which opposite-sign vortices form dipole pairs which propagate through the domain, see [47]. The vanishing inverse temperature at $E = E_m$ corresponds to a homogeneous state with positive and negative vortices spread out evenly over the domain. The point vortex states at different temperatures are summarised in figure 1. Such point vortex states at a given inverse temperature $\beta$ may be generated using the noisy gradient method presented in appendix B, which was previously introduced in [48]. Specifically, once a statistically stationary state is reached, this numerical method generates random point-vortex states according to the canonical distribution associated with the inverse temperature $\beta$. For a given value of $\beta$, the mean energy in the statistically stationary state can be measured from the time series. Thus, like every microcanonical temperature corresponds to an energy $E$ according to (1), in the noisy gradient method every value of $\beta$ corresponds to a mean energy $\langle E \rangle$ in steady state. The resulting mean energy as a function of temperature is shown in figure 2.

## III. THE MODEL

We now describe the simplified model of the interaction of 2-D and 3-D flow studied in this paper. For the sake of simplicity and clarity, the theoretical formalism is presented in the infinite domain. The corresponding equations for the 2-D doubly periodic domain $[0, 2\pi L] \times [0, 2\pi L]$, where the statistical point vortex temperature from section II is well-defined, are given in appendix A.

Consider an even number $N_v$ of point vortices with

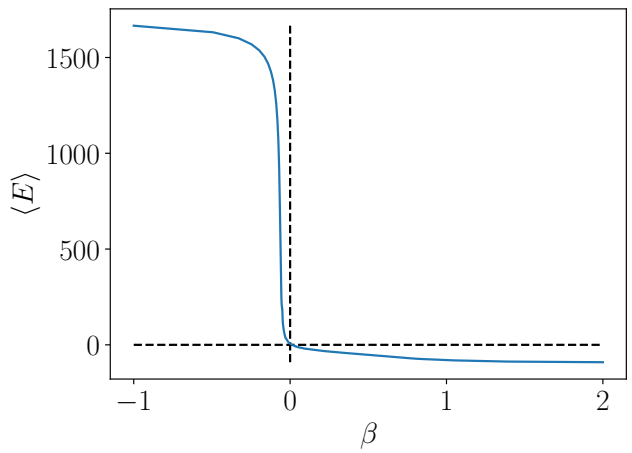


FIG. 2. Mean point vortex energy $\langle E\rangle$ of $N_v = 32$ vortices versus $\beta$, computed using the method described in appendix B in the periodic domain $[0, 2\pi]\times[0, 2\pi]$ (with a truncation at distances smaller than $\epsilon = 0.1$, cf. appendix B). This curve allows a translation from vortex energies at steady state to corresponding temperatures.

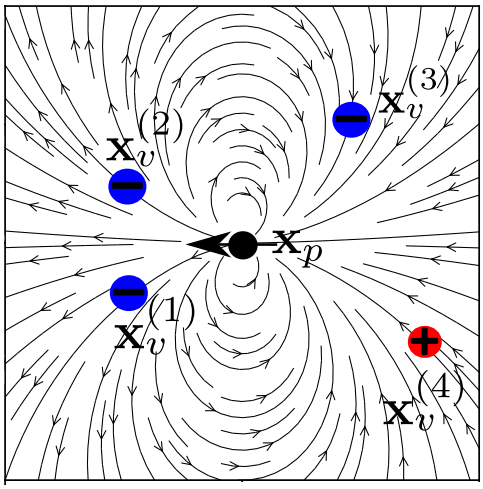


FIG. 3. Illustration of how a velocity field $\mathbf{u}_p$ (steam lines) due to a 3-D perturbation at $\mathbf{x}_p$, can reduce point vortex energy. This is done by increasing the distance between the same-sign vortices at $\mathbf{x}_v^{(1)}, \mathbf{x}_v^{(2)}$ and/or decreasing the distance between opposite-sign vortices at $\mathbf{x}_v^{(3)}, \mathbf{x}_v^{(4)}$. The bold black arrow passing through $\mathbf{x}_p$ represents the dipole moment.

circulations $\Gamma_i$ located at positions $\mathbf{x}_v^{(i)} = (x_v^{(i)}, y_v^{(i)})$. In addition to the point vortices, we introduce localised 3-D perturbations ("*ergophages*"). Motivated by the strong localisation of 3-D motions (spatial intermittency) observed close to the onset of three-dimensionality in simulations [13, 14, 42] we also model 3-D motions as $N_p$ point-like pertubations located at positions $\mathbf{x}_p^{(k)} = (x_p^{(k)}, y_p^{(k)})$. We do not resolve the spatial structure of the perturbations, but rather assign to every ergophage an effective perturbation amplitude $A_k$ (with dimensions of circulation), which measures its intensity. This simplifies the formalism and makes the mathematical structure of the model effectively 2-D.

Point vortices and 3-D point perturbations induce velocity fields that advect each other following the equations

$$\frac{d}{dt}\mathbf{x}_v^{(i)} = \mathbf{U}'^{(i)}_v + \mathbf{U}_p^{(i)} + \mathbf{u}_f^{(i)} \tag{2}$$

and

$$\frac{d}{dt}\mathbf{x}_p^{(k)} = \mathbf{U}_v^{(k)} + \mathbf{v}_f^{(k)} \tag{3}$$

where $\mathbf{U}_v'^{(i)}$ is the velocity induced on vortex $i$ by all point vortices $i \neq j$, $\mathbf{U}_p^{(i)}$ is the velocity induced on vortex $i$ by the 3-D *ergophages* and $\mathbf{U}_v^{(k)}$ is the velocity induced on ergophage $k$ by all $N_v$ point vortices. Finally, $\mathbf{u}_f^{(i)}$ and $\mathbf{v}_f^{(k)}$ are externally imposed velocity fields that could inject energy to the system. Note that ergophages do not advect each other.

In the absence of ergophages and external velocities, point vortices move due to their mutual advection, following Hamiltonian dynamics so that the velocity field $\mathbf{U}'^{(i)}_v$ can be written as

$$\mathbf{U}'^{(i)}_v = \Gamma_i^{-1}\begin{pmatrix}\partial_{y_v^{(i)}} H \\ -\partial_{x_v^{(i)}} H\end{pmatrix}, \tag{4}$$

corresponding to the advection of the $i$-th vortex by all vortices $j \neq i$. The Hamiltonian $H$ in $\mathbb{R}^2$ is given by

$$H(x_v^{(1)}, \ldots, x_v^{(N_v)}) = -\frac{1}{2}\sum_{\substack{i,j=1\\ i\neq j}}^{N_v} \Gamma_i\Gamma_j \log(|\mathbf{x}_v^{(i)} - \mathbf{x}_v^{(j)}|), \tag{5}$$

which is a sum over pairs depending on the vortex-vortex distances alone. The velocity field $\mathbf{U}_v^{(k)}$ closely resembles $\mathbf{U}'^{(i)}_v$, but it includes the advection due to all $N_v$ vortices, formally omitting the condition $i \neq j$ in $H$ before differentiating in (4) and evaluating at $\mathbf{x}_v^{(i)} \to \mathbf{x}_p^{(k)}$. The Hamiltonian also gives the kinetic energy of the flow (up to a factor of $(2\pi)^{-1}$ and an additive infinite constant due to self-energy), which is conserved. The point vortex energy increases when same-sign vortices approach each other and when opposite-sign vortices move apart, while it decreases when same-sign vortices move apart and when opposite-sign vortices approach each other.

In the presence of ergophages, energy of the 2-D field can be transferred to the 3-D field perturbations. Thus, in order to gain energy, an ergophage must reduce the energy of a given point vortex configuration on which it is superimposed. Each ergophage induces a 3-D perturbation velocity field $\mathbf{u}_p^k(\mathbf{x})$ of amplitude $A_k^2$, which has non-zero divergence in the plane. The total velocity field

induced by the ergophages is then given by

$$\mathbf{U}_p(\mathbf{x}) = \sum_{k=1}^{N_p} A_k^2 \mathbf{u}_p^{(k)}(\mathbf{x}), \tag{6}$$

such that the velocity induced on vortex $i$ can be written as $\mathbf{U}_p^{(i)} = \mathbf{U}_p\left(\mathbf{x}_v^{(i)}\right)$. This field modifies the point vortex positions and thus their energy, allowing ergophages to grow under suitable conditions.

Our choice for $\mathbf{u}_p^{(k)}(\mathbf{x})$ should be the simplest possible. It is shown in the appendix D that the choice of a monopole, does suggest itself for its simplicity, would, however, always lead to an amplitude decay of the ergophages. Hence the simplest non-trivial choice for $\mathbf{u}_p^{(k)}(\mathbf{x})$ is given by a dipole field,

$$\mathbf{u}_p^{(k)} = (\hat{d}_k \cdot \nabla) \begin{pmatrix} \partial_x \phi^{(k)} \\ \partial_y \phi^{(k)} \end{pmatrix}. \tag{7}$$

where $\hat{d}_k = (\cos(\varphi_k), \sin(\varphi_k))$ is the dipole moment with $\varphi_k$ the angle between the dipole moment and the $x$-axis. The potential $\phi^{(k)}$ is given by

$$\phi^{(k)}(\mathbf{x}) = -\frac{1}{2} c \log(|\mathbf{x}_p^{(k)} - \mathbf{x}|), \tag{8}$$

where $c$ is a coupling coefficient. An example of dipole interactions is shown in figure 3. In this case the perturbation velocity field makes same-sign vortices approach each other (e.g. $\mathbf{x}_v^{(1)}$ and $\mathbf{x}_v^{(2)}$ in figure 3) and opposite-sign vortices move apart (e.g. $\mathbf{x}_v^{(3)}$ and $\mathbf{x}_v^{(4)}$ in figure 3), thus reducing the point vortex energy. Now, assume one were to exchange $\mathbf{x}_v^{(1)} \leftrightarrow \mathbf{x}_v^{(3)}$ and $\mathbf{x}_v^{(2)} \leftrightarrow \mathbf{x}_v^{(4)}$ in figure 3, keeping $\mathbf{x}_p$ the same. The dipole field would then cause an increase in point vortex energy and thus would no longer lead to any 3-D instabilities. However, it suffices to rotate the dipole moment by 180° to recuperate a 3-D instability. This example illustrates that the dipole field can lead to 3-D instability for a given vortex configuration (even if monopole field would not), provided the the orientation of the dipole moment is suitably chosen. For simplicity the dipole moment in this work will always be chosen such as to ensure maximum energy extraction from the 2-D field.

In our model we assign to the ergophages the energy

$$E_{3D} = \frac{1}{2} \sum_i A_i^2. \tag{9}$$

The energy exchanges between 2-D and 3-D flow must be conservative. Thus any decrease of of the point vortex should correspond to an increase of 3-D ergophage energy. We let the amplitudes $A_k$ evolve according to

$$\frac{\mathrm{d}A_k}{\mathrm{d}t} = (\gamma_k - \nu) A_k - \delta A_k^3 \tag{10}$$

(no implicit summation), where $\gamma_k$ is an instantaneous growth rate due to interactions with the point vortices, $\nu$ (proportional to viscosity) is a linear damping coefficient and $\delta$ is a nonlinear damping coefficient due to self-interactions. In order for the coupling to conserve energy, the growth-rate is given by

$$\gamma_k = -\sum_{i=1}^{N_v} \mathbf{u}_p^{(k)}\left(\mathbf{x}_v^{(i)}\right) \cdot \nabla_{\mathbf{x}_v^{(i)}} H. \tag{11}$$

As is shown in appendix C, these model equations imply that the total energy

$$E_{tot} = H + \frac{1}{2} \sum_{k=1}^{N_p} A_k^2 \equiv H + E_{3D} \tag{12}$$

is conserved, provided $\mu = \delta = 0$ (no dissipation) and $\mathbf{u}_f = \mathbf{0}$ (no energy injection).

In the presence of dissipation it is useful to have an energy injection mechanism as well so that a non-trivial steady state is reached. This is achieved by the choice

$$\mathbf{u}_f^{(i)} = \epsilon_f \left[\nabla_{\mathbf{x}_i} H + |\beta|^{-1/2} \boldsymbol{\eta}_i(t)\right], \tag{13}$$

where $\boldsymbol{\eta}_k(t) = (\eta_k^1(t), \eta_k^2(t))^T$ with independent white Gaussian noise components $\eta_k^i$ satisfying $\langle \eta_k^i(t) \rangle = 0$ and $\langle \eta_k^i \eta_{k'}^{i'} \rangle = 2\delta_{i,i'}\delta_{k,k'}\delta(t-t')$ for the ensemble average $\langle \cdot \rangle$. In the absence of ergophages, this noisy-gradient forcing leads to a point-vortex flow with temperature $\beta^{-1}$ and is described in detail in appendix B.

Finally, since the total energy is independent of the ergophage positions, without changing the energy dynamics we also chose $\mathbf{v}_f$ to be a noise term

$$\mathbf{v}_f^{(k)} = \sigma \boldsymbol{\eta}_k(t) \tag{14}$$

where $\eta_i = (\eta_i^{(1)}, \eta_i^{(2)})$, with $\eta_i^{(j)}$ pairwise independent zero-mean white Gaussian noise terms. The noise is added to eliminate a remaining dependence on initial conditions. Note that in our model, different ergophages do not directly affect each other, neither in terms of their amplitudes, nor their positions. They can only affect each other indirectly by altering the background 2-D flow non-negligibly and thus changing the growth rate $\gamma_k$ experienced by each ergophage.

Equations (2,3,10) define our model that we solve numerically in the sections that follow.

## IV. NUMERICAL IMPLEMENTATION

We developed a fully MPI-parallelized Fortran program, using a fourth-order Runge-Kutta time stepper, to simulate the model in the 2-D doubly periodic domain $[0, 2\pi L] \times [0, 2\pi L]$, based on the Weiss-McWilliams formalism introduced in [49]. The parallelization is implemented by assigning a subset of vortex-vortex pairs and vortex-ergophage pairs to each processor, over which to sum when computing quantities involving such pairs

such as $\mathbf{U}_v^{i)}, \mathbf{U}_p^{(i)}, H$ and $\gamma_k$. The specific model equations for the periodic domain are given in appendix A. Since the periodic domain has a finite area, the statistical point vortex temperature introduced in section II is well-defined here and no vortices can escape to infinity. A regularisation was introduced at distances smaller than a positive cut-off $\epsilon \ll 2\pi L$ (we set $\epsilon/L = 0.1$), similarly as in [33]. The time step $\Delta t$ is dictated by the maximum growth rate $\gamma_k$, which is associated with close encounters where some distances are of the order of $O(\epsilon)$. For highly condensed configurations, where $N_v/2$ vortices form a cluster for each sign of circulation, each cluster comprises approximately $N_v^2/8$ vortex pairs contributing to $\gamma_k$. At small distances $u_p = O(\epsilon^{-2})$ and $\nabla_{\mathbf{x}_v^{(i)}} H = O(\epsilon^{-1})$, such that the time step thus bounded above by

$$\Delta t \lesssim (\max(\gamma_k))^{-1} \sim \frac{8\epsilon^3}{N_v^2}. \tag{15}$$

For dilute vortex configurations, the largest growth rates stem from encounters between a single ergophage and a single vortex, such that $\Delta t \lesssim \epsilon^3$. This strong dependence of the required time step on $\epsilon$, and $N_v$ for dense configurations, is an important limiting factor in computation cost. The operation of the highest numerical complexity at every time step is the evaluation of $\gamma_k$ since it requires summing $O(N_v^2)$ vortex-vortex pairs for every $k = 1, \ldots, N_p$.

## V. SIMULATION RESULTS

To study the model introduced in section III, we first use the noisy gradient method described in appendix B to generate point vortex states with $N_v = 32$ vortices at both positive and negative temperatures. This relatively small number of vortices is chosen in order to be able to run simulations for long times in order to obtain satisfactory statistics. The energy of the resulting equilibria as a function of their inverse temperature $\beta$ is as shown in figure 2. We note that at this relatively low number of vortices, the transitions to a condensate and to pair condensation are not sharp. Using these states as initial conditions for the point vortices, we proceed in the three following steps:

(A) The passive, linear regime: perturbation amplitudes $A_k/\Gamma \ll 1$ and $\delta \to 0$ for a given background point-vortex flow. In this limit, the evolution equation (10) of $A_k$ is linear and the point vortex energy $H$ is constant in time since $\mathbf{U}_p = O(A_k^2)$ is negligible with respect to the conservative Hamiltonian advection terms. To investigate this limit we set $\mathbf{U}_p = 0$ in (3) and $\delta = 0$ in 10. Since there is no dissipation in the system we also set $\mathbf{u}_f = 0$.

(B) The passive, nonlinear regime: still $A_k/\Gamma \ll 1$, such that $H$ still remains unaffected by the 3-D instabilities, but we include saturation of the amplitude $A_k$ due finite $\delta$, i.e. nonlinear self-interaction (in both the linear and passive nonlinear regimes, individual 3-D perturbations evolve independently). In this limit $\mathbf{U}_p = \mathbf{u}_f = 0$ in (3) as well.

(C) The fully nonlinear regime, where the amplitudes $A_k/\Gamma = O(1)$ and thus the induced ergophage velocity on the point vortices $\mathbf{U}_p$ is finite and its effect on point vortices cannot be neglected. In this case $H$ is no longer a system invariant. To sustain the dynamics against dissipation, the "driving" term $\mathbf{u}_f$ given in eq. (13) is included.

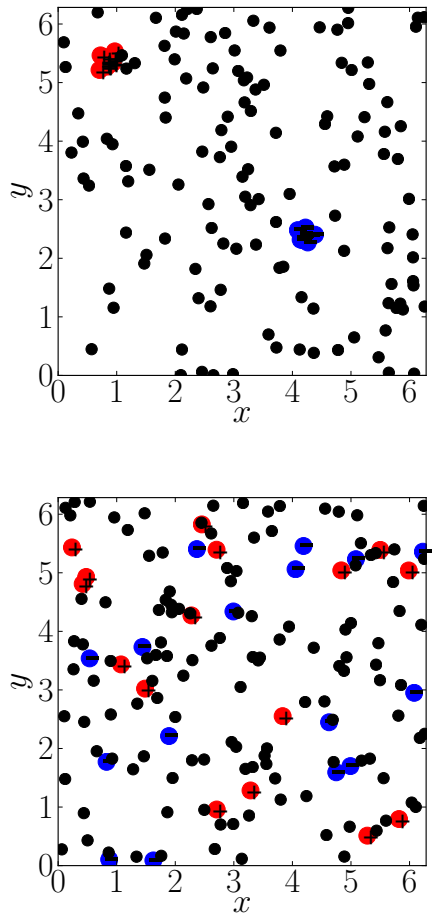


FIG. 4. Snapshots from two simulations with $N_p = 128$ perturbations (black dots) evolving on a point-vortex flow consisting of $N_v = 32$ individual vortices, which is highly condensed at $\beta = -\frac{1}{8}$ (top) and dilute at $\beta = -\frac{1}{128}$ (bottom).

### A. The passive linear regime

We initialise the simulation with $N_v = 32$ vortices at an inverse temperature $\beta$, with half of the vortices having circulation $\Gamma_i = \Gamma$, and the other half having circulation

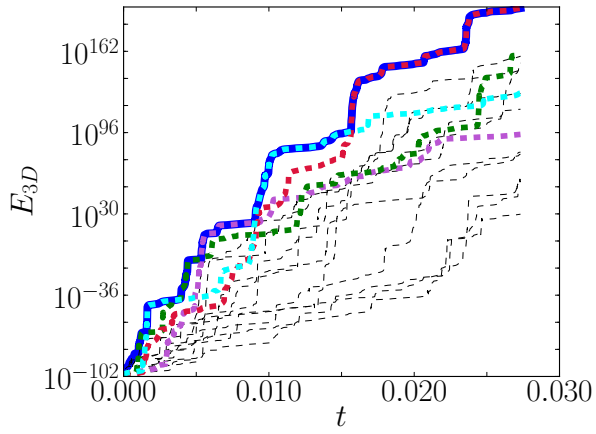


FIG. 5. Lin-log plot showing the time series of the energy of $N_p = 128$ localised 3-D perturbations (total energy shown in solid blue, selected individual contributions $\frac{1}{2}A_k^2$ in dashed black lines) in the passive linear regime with $\nu = 0$, growing on a highly condensed background 2-D flow at $\beta = -\frac{1}{8}$.

$\Gamma_i = -\Gamma$. In addition, we introduce $N_p = 128$ randomly placed ergophages of some small initial amplitude (the same for every perturbation). It is worth reiterating that in the linear phase of the evolution, since there is no feedback on the flow, each ergophage is evolving independently from all the others. Furthermore in the linear phase the effect of the damping parameter $\nu$ is to induce a mean exponential decay. The time evolution of $A_k(t,\nu)$ for any value of $\nu$ can thus be recovered from the $\nu = 0$ case as $A_k(t,\nu) = A_k(t,0)e^{-\nu t}$. For this reason only the $\nu = 0$ case is examined and the growth rate $\gamma'_k$ of a $\nu \neq 0$ case is obtained as $\gamma'_k = \gamma_k - \nu$.

The configuration under study is illustrated in figure 4 for a highly condensed case ($\beta = -\frac{1}{8}$) and a dilute case ($\beta = -\frac{1}{128}$). Then we let the system evolve in time and obtain a time series like the one shown in figure 5 for the highly condensed case, where the 3-D energy (solid blue line) alternates between plateau-like phases of slow growth and phases of abrupt exponential growth. The time series bears resemblance to that obtained from the full linear stability analysis of 3-D instabilities on a turbulent 2-D flow performed by Seshasayanan and Gallet (see fig. 1 in [42]). In the same figure 5, we also show the energy of individual ergophages, $\frac{1}{2}A_k^2$, by dashed lines. Their sum is equal to the blue solid line.

Two important points need to be made. First, one observes in the time evolution of individual ergophages that there are phases of slow or almost zero growth and those of rapid exponential growth. Secondly, at a given time $t$, $E_{3D}(t)$ is dominated by the perturbation with the largest amplitude $A_k(t)$. Abrupt growth events in $E_{3D}$ also occur when another perturbation $A_{k'}$ grows exponentially and "overtakes" $A_k$, thereby leading to abrupt exponential growth of the sum. At every instant $t$, each of the $N_p$ localised perturbations experiences a different growth rate $\gamma_k(t)$, which further varies with time. To understand this linear phase of growth we need to quantify the the statistical properties of these random growth rates.

In figure 6, we plot histograms of $\gamma_k$ sampled over all $k = 1, \ldots, N_p$ and all time steps. In both cases, one observes a power-law range in the PDF. For the dilute case ($\beta = -\frac{1}{128}$) the power-law exponent is close to $-2$ while for the dense state ($\beta = -\frac{1}{8}$) it is closer to $-5/3$. These two exponents can be understood if one identifies the dominant interactions. In the dilute case $|\beta| \ll 1$, where point vortices are far apart, an ergophage maximises its energy extraction when being close to a single point vortex. It does so by moving the point vortex closer to the nearest opposite-sign vortex and/or further apart from the nearest same-sign vortex. In the dense case $-\beta \gg 1$, point vortices are condensed into high-density, same-signed clusters. In order for an ergophage to maximize energy extraction, it needs to be located close to these clusters. Similarly, in the case $\beta \gg 1$ (not demonstrated here) where point-vortex-dipoles are formed, ergophages can only extract energy efficiently if they come close to such dipoles. The PDF of the growth rate $\gamma_k$ can then be calculated by assuming that all positions in space are equally probable and that at each time it is the interaction with the closest pair of point vortices that dominates. A detailed calculation, given in appendix E, leads to the powerlaw

$$P(\gamma) \sim \gamma^{-2} \qquad \text{at large } \gamma. \tag{16}$$

for the dilute limit $|\beta| \ll 1$, while for the dense and point-vortex-dipole $|\beta| \gg 1$ limit one obtains

$$P(\gamma) \sim \gamma^{-5/3} \qquad \text{at large } \gamma. \tag{17}$$

The predicted power laws agree with the PDFs obtained numerically. However, we have to note that in our numerical set-up these results are valid up to a large-$\gamma$ cut-off resulting from the regularisation at distances less than $\epsilon$. This is important because without this regularization, the variance and the mean would be infinite for the power-law PDFs of $\gamma_k$ found here. This implies that some of the results observed here would have an explicit dependence on the choice of this cut-off.

Besides the growth-rate distribution, to characterize the statistical properties of $\gamma_k$ we also need to quantify its auto-correlation time $\tau_{ac}$. We define $\tau_{ac}$ in terms of the normalised auto-correlation function $\Gamma(\tau) = \langle \gamma(t)\gamma(t+\tau)\rangle / \langle \gamma(t)^2 \rangle$, as the smallest $\tau$ for which $\Gamma(\tau) \leq 0.5$, where $\Gamma(0) = 1$ by definition and $\langle \gamma \rangle = \frac{1}{T}\int_0^T dt \sum_{k=1}^{N_p} \gamma_k(t)$ is an average over time $t$ ($T$ is the time at the end of the simulation) and realisations (ergophages). We stress that the small-distance cut-off introduced in the velocity field, leading to a large-$\gamma$ cut-off in $P(\gamma)$ is essential for obtaining a finite mean growth rate $\overline{\gamma}$ and finite noise variance, since a PDF featuring power-law tails with exponents $-2$ and $-5/3$ does not have a finite mean or variance otherwise. Figure 7 shows that the auto-correlation time decreases monotonically with $\sigma$ (defined in equation (14)),

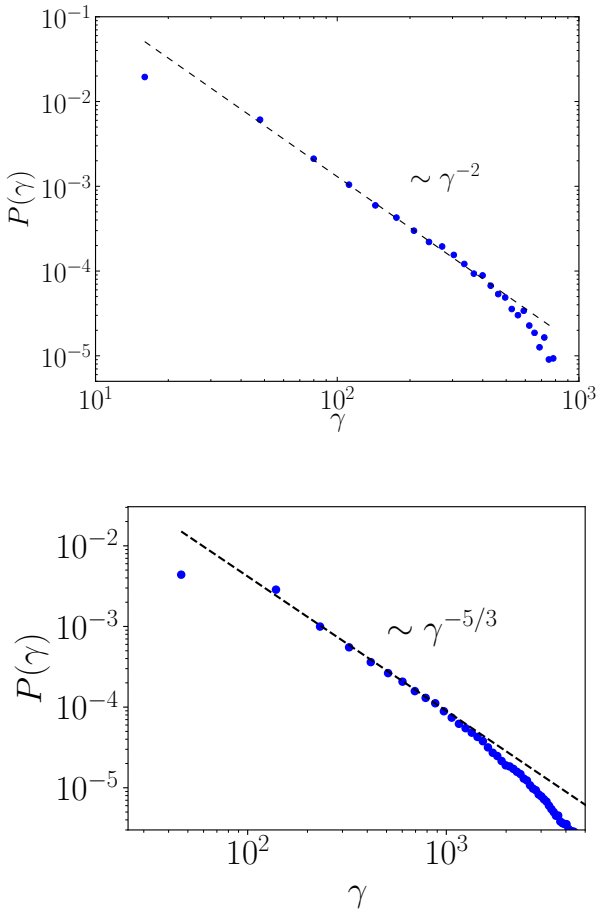


FIG. 6. Two histograms of the growth rate $\gamma_k$, sampled over all time steps and all 128 ergophages from the run corresponding to the two linear simulations with a dilute vortex state at $\beta = -1/128$ (top) and a condensed vortex state at $\beta = -1/8$ (bottom) visualised in figure 4. Power-law ranges with exponents $-2$ and $-5/3$ can be discerned, as predicted for dilute and dense vortex base states, respectively.

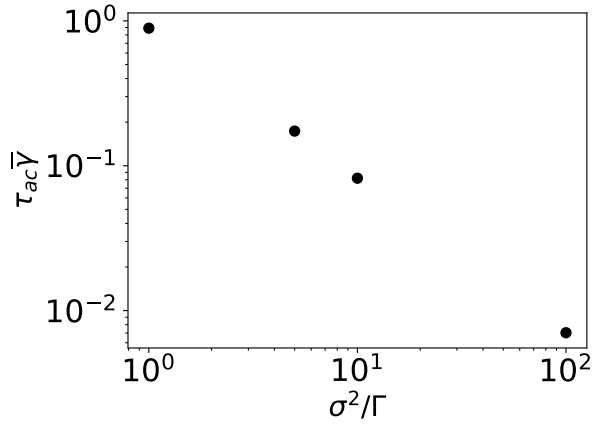


FIG. 7. Log-log plot of the auto-correlation time $\tau_{ac}$ of the growth rate $\gamma$ (see text for the definition of $\tau_{ac}$) in a passive, linear simulation at $\beta = -1/16$, non-dimensionalised by the mean growth rate, versus the squared amplitude of the noise acting on 3-D perturbations, non-dimensionalised by the r.m.s. vortex circulation.

as $\tau_{ac} \sim \sigma^{-2}$. By increasing $\sigma$ sufficiently, one obtains an arbitarily small auto-correlation time. When $\tau_c\overline{\gamma} \ll 1$, then the random process $\gamma_k(t)$ can be approximated as uncorrelated in time.

Summarising the above findings, the length of these steps is randomly distributed according to a PDF with power law tails whose exponents are between $-2$ and $-5/3$ and approximately white in time since it is uncorrelated in time beyond a small correlation time (for sufficently large $\sigma$). These properties imply that the evolution of $A_k$ due to $\gamma_k$ is well approximated by a Lévy flight random process.

A Lévy flight is a random process with independent stationary increments $\eta$, where the increments follow a heavy-tailed PDF. By the generalized central limit theorem [50], the sum of many such heavy-tailed increments follows a Lévy stable PDF $P(\eta; \alpha, \tilde{\beta})$ that depends on two important parameters $\alpha \in (0, 2]$ and $\tilde{\beta} \in [-1, 1]$ [51, 52]. Lévy flights were first introduced by Mandelbrot in [53] and have since found numerous applications, including anomalous diffusion, in particular in fluid turbulence, [50, 54–56], the statistics of 2-D fluid turbulence [57], plasma turbulence [58], finance [59], climatology [60, 61], human mobility [62], COVID-19 spreading [63], animal foraging patterns [64] and more [65, 66]. Bursts with amplitudes following power-law PDFs are also observed in 3-D secondary instabilities for zero-Prandtl-number convection [67, 68]. The influence of the parameters $\alpha, \tilde{\beta}$ on the distribution $P(\eta)$ is as follows. For $\alpha = 2$, one obtains the Gaussian distribution. For $1 \leq \alpha < 2$, a stable distribution features a power-law tail $P(\eta) \sim \eta^{-\alpha-1}$ at $|\eta| \to \infty$. The parameter $\tilde{\beta}$ measures the asymmetry of PDF, with $\tilde{\beta} = 0$ corresponding to a symmetric PDF and $|\beta| = 1$ corresponding to a maximally asymmetric PDF. In the particular case of $\beta = 1$ and $\alpha < 1$, one obtains a one-sided PDF with support on $\mathbb{R}_+$ only.

If $\gamma_k$ is then interpreted as Lévy noise, equation (10) is a stochastic equation with multiplicative Lévy noise whose parameters depend on the 2-D flow temperature. The dense and dilute cases described above, for which the $\gamma_k$ PDF has power law ranges with exponents $-5/3$ and $-2$, respectively, correspond to noise parameters $\alpha = 2/3$ and $\alpha = 1$, respectively, and $\tilde{\beta} = 1$ since the linear growth rate $\gamma_k$ is always positive in the model by construction.

The dynamical behavior of systems with multiplicative Gaussian white noise has found a plethora of applications, in particular to the phenomenon of on-off intermittency [69–71]. While the role of long-time correlated noise in on-off intermittency has been considered before [72–75], the case of on-off intermittency with heavy-tailed

noise has not previously been studied explicitly, to our knowledge. Our companion paper [1] is devoted to this topic. Here we summarize only the relevant results. It is shown in [1] that in the case $\alpha < 1$ and $\tilde{\beta} = 1$ which applies here, the system (10), with $\gamma_k$ interpreted as white Lévy noise, is unstable for all values of $\nu$: since the mean value of $\langle \gamma_k \rangle \to +\infty$, viscosity $\nu$, no matter how large, cannot stop the growth of $A_k$. If, however, the attained values of $\gamma_k$ are truncated, so that a finite value of $\langle \gamma_k \rangle$ exists, then there is a critical value of viscosity $\nu_c$ above which all trajectories converge to zero $A_k \to 0$. However, this critical value depends on the truncation value of $\gamma_k$, which in the problem at hand implies that the $\nu_c$ will depend on the regularization cut-off $\epsilon$. At long time scales the system displays on-off intermittency.

### B. The passive nonlinear regime

We solve the model equations for $N_p = 32$ passive nonlinear dipole ergophages evolving on a highly condensed background flow of $N_v = 32$ point vortices at temperature $\beta = -1/8$, fixing the nonlinear damping coefficient at $\delta = 1$. For a given $\nu$, we initialise the ergophages at random positions and with small amplitudes. We let the system evolve for long times, such that the perturbation amplitude either decays or reaches a statistically steady state. We then measure the steady-state time average of the moments $M_n = \langle A^n \rangle$, in terms of $\langle f(A) \rangle = \lim_{T\to\infty} \frac{1}{TN_p} \int_0^T \sum_{k=1}^{N_p} f(A_k) dt$. We also define the "zeroth" moment as $M_0 = \exp(\langle \log(A) \rangle)$, By the inequality of arithmetic and geometric means the moments are ordered $M_0 \le M_1 \le M_2^{1/2} \le M_3^{1/3} \le \dots$. The resulting bifurcation diagram of $M_0, M_1, M_2$ as a function of $\nu$ is shown in figure 8.

On-off intermittency predicts that all non-zero moments scale linearly with $\nu_c - \nu$, $M_n \propto (\nu_c - \nu)$, while the zeroth moment scales as $M_0 \propto \exp(-cst./(\nu_c - \nu))$. Comparing this with figure 8, where the scalings from the Gaussian case are shown by dashed lines, one sees that the time-averaged moments and the Gaussian scalings agree well within the errorbars. This is a consequence of the truncation in the model, which subjects the statistics to a convergence to the Gaussian case, albeit "ultraslow" [76], by the central limit theorem after the sample averaging and/or long-time averaging procedures.

Another prediction of on-off intermittency is that the PDF of the unstable field shows an integrable powerlaw divergence at zero amplitude with an exponent that approaches the value -1 from above as $\nu \to \nu_c$, while an exponential cut-off is expected for large values of $A_k$. Figure 9 shows the PDF of $A_k$. At small values of $A$ the PDF displays a power law $A^\kappa$ with $\kappa$ approaching -1 as $\nu \to \nu_c$ in agreement with the Gaussian on-off prediction. At large $A$ the PDF shows a steeper power-law scaling. In the companion paper [1], the asymptotics $P(A) \propto A^{-3} \log^{-2/3}(A)$ at large values of $A$ are found

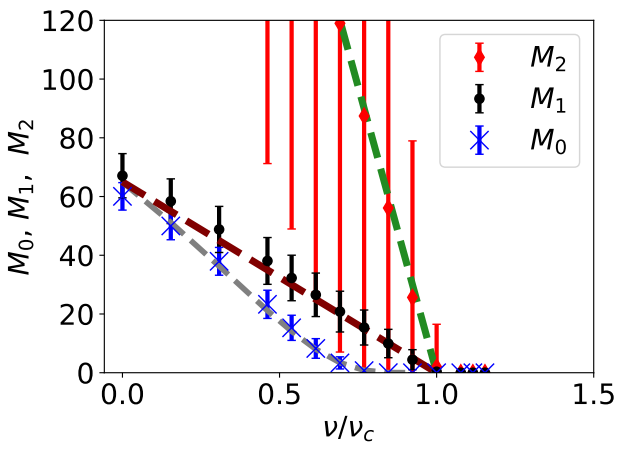


FIG. 8. Bifurcation diagram for $N_p = 32$ passive nonlinear (i.e. independent) dipole ergophages on the background flow at $\beta = -1/8$, $\delta = 1$. The values of $\langle X \rangle_n$ is averaged over the statistically steady state. Error bars are given by the sample standard deviation of the time series in steady state. The dashed lines show the scalings from the Gaussian noise case.

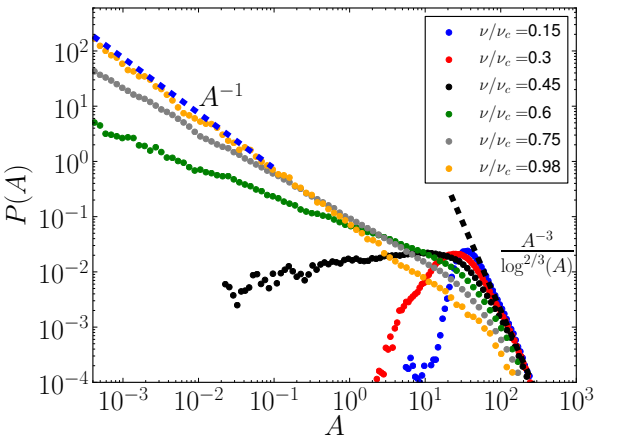


FIG. 9. Steady state PDF of ergophage amplitudes from the numerical solution of the model in the passive nonlinear regime for $\delta = 1$, $\nu/\nu_c = 0.15$ on the background flow at $\beta = -1/8$.

analytically from a fractional Fokker-Planck equation for non-truncated multiplicative Lévy noise with parameters $\alpha = 2/3$, $\beta = 1$ in a quartic potential (in the Stratonovich interpretation), which fits the present data well. Since $A^{-1} \log^{-\alpha}(A)$ is only integrable at $A \to \infty$ for $\alpha > 1$, the scaling $P(A) \propto A^{-3} \log^{-2/3}(A)$ implies that without a cut-off, only the mean is finite, while the variance and all higher moments diverge. With a cut-off at length $\epsilon$, all moments are finite, but only the mean is of order one, while all higher moments depend on the cut-off value $\epsilon$, increasing as the latter is decreased. This is an important difference from the Gaussian noise case. We

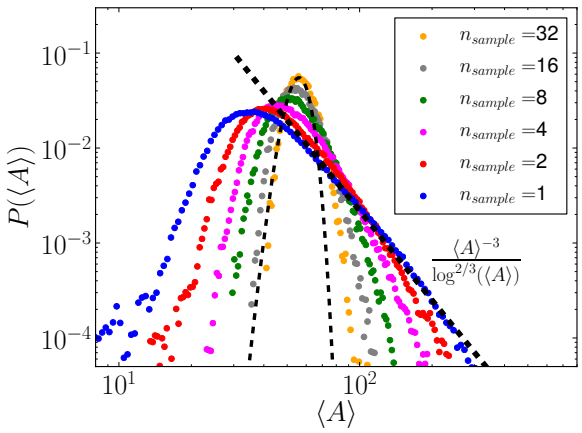


FIG. 10. PDF of sample mean $\langle A\rangle$, over $n_{sample}$ realisations (independent ergophages) from the passive nonlinear point vortex model with parameters $\delta = 1$, $\nu/\nu_c = 0.15$. For $n_{sample} = 1$, the PDF is close to the theoretical prediction for the non-truncated system, and converges to a Gaussian PDF (thin dashed line) as $n_{sample}$ is increased.

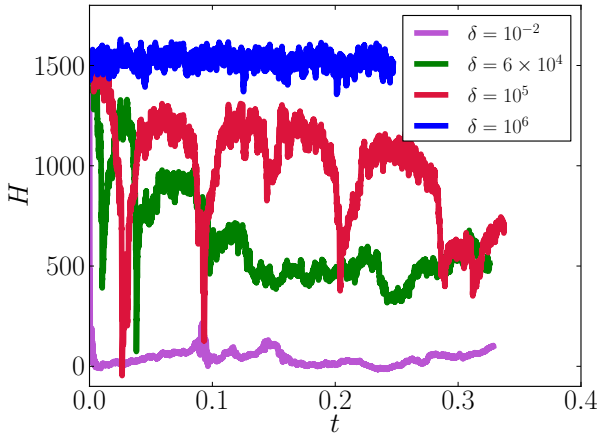


FIG. 11. Time series of the 2-D energy $H$ in the fully nonlinear regime at $\nu/\nu_c = 0.15$ for different values of $\delta$. At $\delta = 10^5$, the flow is close to a 2-D condensate, up to abrupt events when the condensate is disrupted. For decreasing values of $\delta$, ergophages grow to larger amplitudes and lower the energy of the 2-D flow further.

note, however, that this difference is diminished as larger samples are used due to the imposed truncation and the law of large numbers. This is demonstrated in figure 10 which focuses on this power-law tail far from threshold $\nu/\nu_c = 0.15$, and averaging $A$ over independent samples leads to a convergence towards a Gaussian distribution. For a single realisation, however, we observe a form close to the theoretical prediction for the non-truncated Lévy process.

### C. The fully nonlinear regime

We now enable ergophages to feed back on the point-vortex flow and include the driving velocity $\mathbf{u}_f$. Initialising a simulation at a condensed vortex state with $\beta = -1/8$, $N_p = 32$ ergophages at random locations with small initial amplitudes $A_k$ for given values of $\nu, \delta$ and using a forcing temperature $\beta_f = -1/8$, we let the system evolve in time and measure the mean energy around which the energy fluctuates at late times.

Figure 11 shows time series of the 2-D energy $H$ in the fully nonlinear regime for $\nu/\nu_c = 0.15$ for different values of $\delta$. For large $\delta = 10^6$, the 3-D instabilities cannot grow to large amplitudes and therefore do not disrupt the highly energetic condensate. For $\delta = 10^5$, a slightly less energetic condensate persists, but is disrupted at random times by catastrophic events that bring the 2-D flow energy close to zero, just to rebuild again thanks to the driving. These are the traces of the jumps due to Lévy flight dynamics remaining present in the nonlinear regime. Disruptive events occur when an ergophage comes very close to the point vortex clusters shown in the top panel of figure 4, extracting the cluster's energy

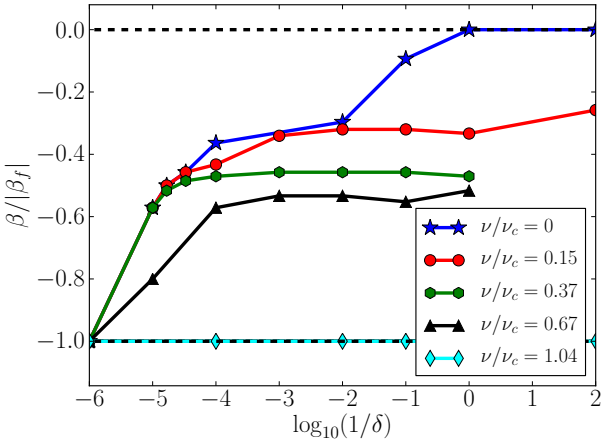


FIG. 12. Plot of mean temperature of the point vortex flow in a fully nonlinear regime in the presence of a single perturbation $N_p = 1$ for varying $\delta$, different curves show different $\nu$. At $\nu/\nu_c > 1$, the flow temperature is exactly that of the forcing, i.e. $\beta = \beta_f = -1/8$, since all 3-D perturbations decay.

by partially breaking it up. With decreasing values of $\delta$, the ergophages disrupt the condensate further and further until they reduce its energy to close to zero driving all point vortices apart.

For each simulation, we use the correspondence between mean energy and inverse temperature visualised in figure 2 to assign a vortex temperature based on the measured average point-vortex energy at late times. We repeat this procedure for several values of $\nu$ and $\delta$ to obtain the diagram shown in figure 12. For $\nu/\nu_c > 1$, 3-D perturbations decay and the 2-D condensate is stable for

all values of $\delta$. For $\nu/\nu_c < 1$, $\beta$ increases with decreasing $\delta$. For smaller values of $\delta$, the perturbation amplitudes saturate at larger values, thus disrupting the 2-D condensate more strongly. When $\delta$ is small enough, the 2-D flow reaches $\beta = 0$, which corresponds to a total disruption of the condensate. For $\nu = 0$, this occurs at $\delta = 1$. Since the energy-$\beta$ curve shown in figure 2 is very steep at small energies, small deviations in the energy do not necessarily correspond to vanishing $\beta$. Furthermore we note that positive values $\beta$ induced by the ergophagues were never observed.

In summary, the 2-D vortex temperatures depend on the linear and nonlinear damping coefficients of the 3-D flow, ranging from a stable condensate to a complete disruption of the latter. The jumpy Lévy flight dynamics discussed for of the linear and weakly nonlinear regimes traces through to the nonlinear regime, and shows in the time series in figure 11 by a random disruption of the 2-D condensate followed by a rapid subsequent rebuilding of the latter due to the driving.

## VI. CONCLUSIONS

We have formulated and analysed a point-vortex model of localised three-dimensional instabilities on two-dimensional flows. Although the coupling of the 3D perturbations in the model is ad-hoc not stemming directly from the Navier-Stokes equations, it has some attractive properties being energy conserving and reducing to the classical point vortex model in certain limits. Most importantly however, it has lead to some very interesting behaviors and predictions that could apply to more realistic quasi-two-dimensional systems exhibiting spectral condensation.

First of all the model predicts fluctuating growth rates with power-law tails, which lead to a Lévy flight in (logarithmic) perturbation amplitude. This suggests a simple explanation for recent DNS results [42] indicating abrupt, jump-like growth of 3-D instabilities on a turbulent 2-D flow. Furthermore the model suggests that the onset of the instability depends on the regularisation cut-off $\epsilon$. For realistic simulations of quasi-two dimensional flows this would imply that the onset of 3-D instabilities would depend on properties measured at the core of the observed vortices that could differ by order of magnitude from mean values.

A new type of intermittency near the onset of an instability was discovered. The corresponding situation of on-off intermittency in the presence of Lévy noise either untruncated or truncated at very large noise amplitudes, is discussed in the companion paper [1].

In the passive nonlinear regime of the model, we observed a continuous transition from finite to vanishing 3-D amplitudes, with on-off intermittent behaviour close to onset. However, a deviation from the Gaussian was observed at large values of the ergophage amplitude, in the form of a power-law tail whose exponent matches theoretical predictions derived from a fractional Fokker-Planck equation in the companion paper [1]. This exponent also implies that the saturation amplitude of the second and higher moments would depend on the regularisation cut-off $\epsilon$ but not the mean.

In the fully nonlinear, strongly coupled regime, where the vortex temperature is affected by the presence of perturbations, we characterised the dependence of vortex temperature on the ergophage damping coefficients and showed that at large amplitude of the 3-D perturbations this temperature reduces to zero. We also showed that at intermediate values of the parameters $\delta$ and $\nu$, a highly energetic condensate, present when 3-D perturbations are small, is disrupted at random times by catastrophic events where 3-D perturbations grow and the condensate amplitude is reduced to very small values, after which it recovers. Such events have also been observed in simulations of thin-layer and rotating flows [14, 42, 77].

In view of the limitations of existing theories, our model provides new a new perspective on 3-D instabilities growing on 2-D flows, which will be useful in analysing and understanding the much more complex results of DNS and potentially guide further theoretical developments.

## ACKNOWLEDGMENTS

This work was granted access to the HPC resources of MesoPSL financed by the Region Ile de France and the project Equip@Meso (reference ANR-10-EQPX-29-01) of the programme Investissements d'Avenir supervised by the Agence Nationale pour la Recherche and the HPC resources of GENCI-TGCC & GENCI-CINES (Projects No. A0070506421, A0080511423, A0090506421 ) where the present numerical simulations have been performed. This work has also been supported by the Agence nationale de la recherche (ANR DYSTURB project No. ANR-17-CE30-0004). AvK acknowledges support by Studienstiftung des deutschen Volkes.

### Appendix A: The model equations for periodic boundary conditions

In the main text, the model is presented in infinite space for clarity. Here, we describe the case of 2-D doubly periodic domain $[0, 2\pi L] \times [0, 2\pi L]$, in which an overall neutral set of an even number $N_v$ of point vortices with circulations $\Gamma_n = (-1)^n \Gamma$, located at positions $\mathbf{x}_v^{(i)} = \left(x_v^{(i)}, y_v^{(i)}\right)$ move due to their mutual advection. We describe this configuration using the Weiss-McWilliams formalism introduced in [49]. In addition, as in the main text, we introduce to $N_p$ localised 3-D perturbations ("ergophages"), idealised as being point-like, at positions $\mathbf{x}_p^{(k)} = \left(x_p^{(k)}, y_p^{(k)}\right)$, which are advected by

the 2-D point vortex motions through the 2-D domain, and whose amplitude $A_k$ may grow by extracting energy from the 2-D flow.

### 1. Equations of motion and Hamiltonian

The equations of motion of the point vortices and ergophages in the periodic domain are given by the same equations as in the infinite space, (2) and (3) along with (4). The Hamiltonian in the periodic domain differs from that in the infinite plane, and is given by

$$H(\{\mathbf{x}_v^{(i)} - \mathbf{x}_v^{(j)}\}) = -\frac{1}{2}\sum_{\substack{i,j=1\\ i\neq j}}^{N_v} \Gamma_i\Gamma_j h(\mathbf{x}_v^{(i)} - \mathbf{x}_v^{(j)}), \quad \text{(A1)}$$

with $\mathbf{x}_{vv}^{ij} \equiv \mathbf{x}_v^{(i)} - \mathbf{x}_v^{(j)} \equiv (x_{vv}^{ij}, y_{vv}^{ij})$ and the vortex-pair energy function in the periodic domain given by

$$h(x,y) = \sum_{m=-\infty}^{\infty} \ln\left(\frac{\cosh(x/L - 2\pi m) - \cos(y/L)}{\cosh(2\pi m)}\right) - \frac{x^2}{2\pi L^2}, \quad \text{(A2)}$$

where the infinite sum over $m$ stems from the sum over all copies of the periodic domain, as shown in [49]. A useful alternative notation for the 2-D point vortex advection is given in [49] as

$$\Gamma_i^{-1}\begin{pmatrix} +\partial_{y_v^{(i)}} H \\ -\partial_{x_v^{(i)}} H \end{pmatrix} = \sum_{\substack{j=1\\ j\neq i}}^{N_v} \Gamma_j \begin{pmatrix} -S\left(y_{vv}^{ij}, x_{vv}^{ij}\right) \\ +S\left(x_{vv}^{ij}, y_{vv}^{ij}\right) \end{pmatrix}, \quad \text{(A3)}$$

in terms of the rapidly converging series

$$S(x,y) = \sum_{m=-\infty}^{\infty} \frac{\sin(x/L)}{\cosh(y/L - 2\pi m) - \cos(x/L)}. \quad \text{(A4)}$$

Equation (A3) relies on the identities $\partial h/\partial x(x,y) = S(x,y) = \partial h/\partial y(y,x)$. We note that at small distances, the periodic copies are negligible and one recovers the results valid in the infinite plane. In particular, for $x, y \ll 1$, $S(x,y) \approx xL/(x^2+y^2)$. This enables us to transfer all results pertaining to small distances in the infinite plane to the periodic case.

### 2. Interactions

As in the main text, each of the localised 3-D perturbations is assigned an amplitude $A_k \geq 0$, $k = 1, \ldots, N_p$, with an associated energy $A_k^2/2$, such that the total energy is again given by (12), with $H$ given by (A1). For the velocity $\mathbf{U}_p^{(i)}$ induced by the ergophages on the point vortices, we choose again the form given in equation (6). The expression for the dipole field given in equations (7) and (8) must be adapted to satisfy the periodic boundary conditions. This is done by tiling $\mathbb{R}^2$ with infinitely many copies of the domain $[0, 2\pi L]\times[0, 2\pi L]$ and summing over all copies. For a periodic monopole, one obtains

$$\mathbf{u}_{p,monopole}^{(k)}(\mathbf{x}) = \nabla\phi^k(\mathbf{x}), \quad \text{(A5)}$$

where the potential $\phi^k$, is given by

$$\phi_k(\mathbf{x}) = h\left(x - x_p^{(k)}, y - y_p^{(k)}\right), \quad \text{(A6)}$$

in terms of the vortex-pair energy function $h(x,y)$ defined in (A2). The dipole field arises from the difference between two monopoles at small distances, and it is therefore equal to the derivative of the monopole field along the dipole moment $\hat{d}_k = (\cos(\varphi_k), \sin(\varphi_k))$,

$$\mathbf{u}_p^{(k)}(\mathbf{x}) = (\hat{d}\cdot\nabla_{\mathbf{x}})\mathbf{u}_{p,monopole}^{(k)}(\mathbf{x}) \quad \text{(A7)}$$

As in the main text, if the $A_k$ obey (10) with $\gamma_k$ given by (11), then the total energy is conserved in time for arbitrary $\hat{\mathbf{u}}_p$, provided that $\mu = \delta = 0$ (no dissipation), and $\mathbf{u}_f = 0$.

The dipole phase $\varphi_k$ is an important degree of freedom, which can be adjusted for sustained growth of ergophage amplitude. Indeed, one can rewrite the growth rate as

$$\gamma_k = \Theta_k\cos(\varphi_k) + \Sigma_k\sin(\varphi_k), \quad \text{(A8)}$$

with

$$\Theta_k = -\sum_{i=1}^{N_v}\left(\frac{\partial^2\phi_k(\mathbf{x}_v^{(i)})}{\left(\partial x_v^{(i)}\right)^2}\frac{\partial H}{\partial x_v^{(i)}} + \frac{\partial^2\phi_k(\mathbf{x}_v^{(i)})}{\partial x_v^{(i)}\partial y_v^{(i)}}\frac{\partial H}{\partial y_v^{(i)}}\right) \quad \text{(A9)}$$

and

$$\Sigma_k = -\sum_{i=1}^{N_v}\left(\frac{\partial^2\phi_k(\mathbf{x}_v^{(i)})}{\partial x_v^{(i)}\partial y_v^{(i)}}\frac{\partial H}{\partial x_v^{(i)}} + \frac{\partial^2\phi_k(\mathbf{x}_v^{(i)})}{\left(\partial y_v^{(i)}\right)^2}\frac{\partial H}{\partial y_v^{(i)}}\right). \quad \text{(A10)}$$

The form of (A8) implies that for any vortex configuration, there is an optimum value of the phases $\varphi_k$, for which the growth rate $\gamma_k$ is at its (positive) maximum, is given by

$$\varphi_k^* = \arctan\left(|\Sigma_k/\Omega_k|\right), \quad \text{(A11)}$$

The above formulae also apply to dipole ergophages in the infinite domain with the potential (8). We let $\varphi_k = \varphi_k^*$ for all $k$ at every instant, implying growth of 3-D instabilities in the inviscid case.

### 3. Numerical implementation of the model

We implemented the equations corresponding to (2, 3, 10) with (A7) and (A11) in a fully MPI-parallelized

Fortran program using a fourth-order Runge-Kutta time stepper. For the numerical implementation, a regularisation was introduced at distances smaller than $\epsilon \ll 2\pi L$, for $\epsilon > 0$, in a manner inspired by [33]. Specifically, we replace

$$h(x,y) \to \sum_{m=-\infty}^{\infty} \ln\left(\frac{\cosh\left(\frac{x-2\pi mL}{L}\right) - \cos\left(\frac{y}{L}\right) + \epsilon^2}{\cosh(2\pi m)}\right) - \frac{x^2}{2\pi L^2} \tag{A12}$$

and

$$S(x,y) \to \sum_{m=-\infty}^{\infty} \frac{\sin(x/L)}{\cosh(y/L - 2\pi m) - \cos(y/L) + \epsilon^2}. \tag{A13}$$

As mentioned in the main text, the parallelization is implemented straightforwardly by splitting up the sums over vortex-vortex pairs and vortex-parasite pairs into chunks, each of which is assigned to one processor. The choice of the time step is discussed in the main text.

## Appendix B: Method for generating point vortex configurations at a given temperature

Consider $N$ point vortices located at positions $(x_i, y_i)$, $i = 1, \ldots, N$ in a given finite domain, with associated Hamiltonian $H$. Pick a positive or negative temperature $T \in \mathbb{R}$. Consider the stochastic gradient dynamics defined by

$$\frac{\mathrm{d}x_i}{\mathrm{d}t} = -\mathrm{sgn}(T)\frac{\partial H}{\partial x_i} + \sqrt{k_B|T|}\eta_i^{(1)}(t), \tag{B1}$$

$$\frac{\mathrm{d}y_i}{\mathrm{d}t} = -\mathrm{sgn}(T)\frac{\partial H}{\partial y_i} + \sqrt{k_B|T|}\eta_i^{(2)}(t). \tag{B2}$$

where $\eta_i^{(1)}(t)$ and $\eta_i^{(2)}(t)$ are pairwise independent delta correlated Gaussian noise terms, i.e. $\langle \eta_i^{(1)} \rangle = \langle \eta_i^{(2)} \rangle = 0$ and $\langle \eta_i^{(j)}(t)\eta_{i'}^{(j')}(t') \rangle = 2\delta(t-t')\delta_{i,i'}\delta_{j,j'}$, in terms of the ensemble average $\langle \cdot \rangle$. Denote by $\mathbf{X}$ the state vector with entries $X_{2n-1} = x_n$, $X_{2n} = y_n$ for $n = 1, \ldots, N$. Further, let $\nabla_{\mathbf{X}}$ denote the $2N$-dimensional gradient operator with respect to $\mathbf{X}$, then the Fokker-Planck equation for the probability density $P(\mathbf{X}, t)$ associated with the given gradient dynamics reads

$$\partial_t P = \nabla_{\mathbf{X}} \cdot \mathbf{F}, \quad \text{where} \quad \mathbf{F} = \mathrm{sgn}(T)(\nabla_{\mathbf{X}} H)P + k_B|T|\nabla_{\mathbf{X}} P. \tag{B3}$$

In steady state, the flux of probability vanishes if there is no absorption or injection of probability at the boundaries. Solving the zero-flux condition gives the stationary probability density $P_s(\mathbf{X})$

$$P_s(\mathbf{X}) = \frac{1}{Z}\exp\left(-\frac{H(\mathbf{X})}{k_B T}\right), \tag{B4}$$

which is the Boltzmann equilibrium distribution of the system at temperature $T$. Thus, solving equations (B1, B2) numerically, the system reaches a steady state which is precisely the equilibrium at temperature $T$. Importantly, adding the Hamiltonian advection term $U_v^{(i)}$ as in (2) does not change this equilibrium, since the associated terms in the Fokker-Planck equation cancel for every index $i$ (being the divergence of a curl).

## Appendix C: Conservaton of energy

For the evolution equations (2, 10, 11), for $\mu = \delta = 0$ and no forcing, one finds that the total energy is conserved, since

$$\frac{\mathrm{d}E_{tot}}{\mathrm{d}t} = \frac{dH}{dt} + \sum_{k=1}^{N_p} A_k \frac{dA_k}{dt} \tag{C1}$$

$$= \sum_{i=1}^{N_v} \mathbf{U}_p^{(i)} \cdot \nabla_{\mathbf{x}_v^{(i)}} H + \sum_{k=1}^{N_p} A_k(\gamma_k A_k) \tag{C2}$$

$$= \sum_{i=1}^{N_v}\sum_{k=1}^{N_p} A_k^2 \mathbf{u}_p^{(k)}(\mathbf{x}_v^{(i)}) \cdot \nabla_{\mathbf{x}_v^{(i)}} H - \sum_{k=1}^{N_p}\sum_{i=1}^{N_v} A_k^2 \mathbf{u}_p^{(k)}(\mathbf{x}_v^{(i)}) \cdot \nabla_{\mathbf{x}_v^{(i)}} H \tag{C3}$$

$$= 0 \tag{C4}$$

This conservation of energy is independent of the modelling choice of the velocity field $\mathbf{u}_p$ and of the particular form of the Hamiltonian. Hence the conservation holds for arbitrary boundary conditions.

## Appendix D: Vanishing mean growth rate for monopole 3-D perturbations and derivation of dipole formulas

The simplest possible choice for the velocity induced by 3-D perturbations, $\mathbf{u}_p(\mathbf{x})$, in infinite space is an isotropic radial profile,

$$\mathbf{u}_p^{(k)}(\mathbf{x}) = \frac{\mathbf{x} - \mathbf{x}_p^{(k)}}{|\mathbf{x} - \mathbf{x}_p^{(k)}|^2}, \tag{D1}$$

i.e. a monopole profile. Since it decays at infinity, it is admissible in the infinite plane. In a periodic domain, however, it needs to be adapted to the boundary conditions by summing over an infinite grid of images:

$$\mathbf{u}_p(\mathbf{x})^{(k)} = \sum_{n,m=-\infty}^{\infty} \frac{\mathbf{x} - \mathbf{x}_p^{(k)} - \begin{pmatrix} 2\pi n \\ 2\pi m \end{pmatrix}}{\left|\mathbf{x} - \mathbf{x}_p^{(k)} - \begin{pmatrix} 2\pi nL \\ 2\pi mL \end{pmatrix}\right|^2} = \begin{pmatrix} S(x - x_p^{(k)}, y - y_p^{(k)}) \\ S(y - y_p^{(k)}, x - x_p^{(k)}) \end{pmatrix}, \tag{D2}$$

where $S(x,y)$ is as defined by the rapidly converging series given in (A4) and regularised in (A13). Equation (D2) provides an alternative expression for the periodic monopole field, equivalent to that in (A6) We note that the infinite sum is exactly the double series calculated by Weiss and McWilliams in [49]. The corresponding growth rate of perturbation $k$ given in (11) can be rewritten as

$$\gamma_k = \frac{c}{2} \sum_{\substack{i,j=1 \\ i \neq j}}^{N_p} \Gamma_i \Gamma_j \nabla h|_{\mathbf{x}_{vv}^{ij}} \cdot \left( \nabla h|_{\mathbf{x}_{vp}^{ik}} - \nabla h|_{\mathbf{x}_{vp}^{jk}} \right) \tag{D3}$$

with $\mathbf{x}_{vv}^{ij} = \mathbf{x}_v^{(i)} - \mathbf{x}_v^{(j)}$ and $\mathbf{x}_{vp}^{ik} = \mathbf{x}_v^{(i)} - \mathbf{x}_p^{(k)}$. It has been used that from eq. (A4) that $\partial h/\partial x(x,y) = S(x,y) = \partial h/\partial y(y,x)$. For simplicity, since the sum is over vortex pairs, consider a single such pair with circulations $\Gamma_1, \Gamma_2$ at arbitrary positions $\mathbf{x}_1, \mathbf{x}_2$. Place a single ergophage at position $(x,y)$. The sum over $i,j$ in (D3) reduces to a single term. Applying the averaging operator over ergophage positions,

$$\overline{F} \equiv \frac{1}{4\pi^2 L^2} \int_0^{2\pi L} \int_0^{2\pi L} F(x,y) dx dy,$$

to the growth rate gives zero, since $h$ is $2\pi L$-periodic in both the $x$ and $y$ directions. We conclude that the mean growth rate of a monopole ergophage due to a single vortex pair vanishes, for arbitrary vortex positions. Thus the mean total ergophage growth rate, being the sum of pair contributions, also vanishes. Assuming that for a given vortex configuration, all ergophage positions are equally likely, then the resulting mean growth rate vanishes in the absence of dissipation. When dissipation is added, then 3-D perturbations must decay at long times. This is illustrated by a long run with $N_p = 32$ passive nonlinear monopole ergophages and $N_v = 32$ point vortices in figure 13. Therefore, the monopole model is insufficient and the dipole model suggests itself as having the minimal complexity to capture mean growth of 3-D perturbations.

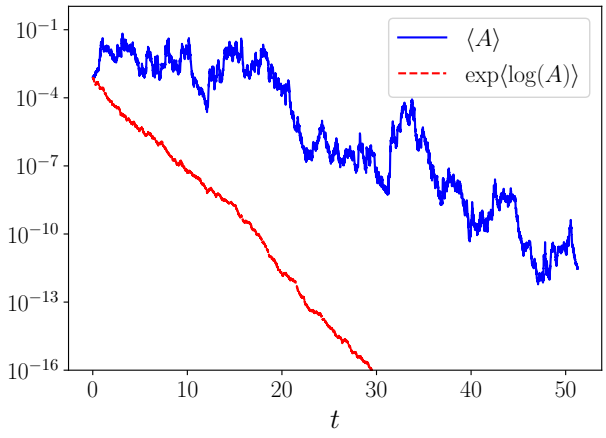


FIG. 13. Lin-log plot of the time series of the first moment $M_1 = \langle A \rangle$ and the zeroth moment $M_0 = \exp(\langle \log(A) \rangle)$ of ergophage amplitude, in terms of the sample average $\langle f(A) \rangle = \frac{1}{N_p} \sum_k f(A_k)$, from a passive nonlinear simulation with $N_p = 32$ ergophages inducing a monopole field, experiencing disspation $\nu, \delta > 0$. The zeroth moment decays exponentially, indicating that the mean growth rate is negative. Both moments clearly decay at late times as predicted theoretically.

## Appendix E: Power laws in growth rate probability density

For the dipole parasites introduced in the main text, consider the growth rate of the amplitude of a given ergophage at location $\mathbf{x}_p$, associated with a vortex pair of circulation $\Gamma_1, \Gamma_2$ at positions $\mathbf{x}_1 = (\ell/2, 0), \mathbf{x}_2 = (-\ell/2, 0)$. We are interested in the tails of the probability density function (PDF), where the ergophage is very close to one or several point vortices, hence boundary conditions are irrelevant and we perform the analysis in the infinite plane. The localised perturbation has a dipole moment $\hat{d} = (\cos(\varphi), \sin(\varphi))$ attached to it as well as an amplitude $A$, whose growth rate is given by

$$\gamma = \frac{\Gamma_1 \Gamma_2}{\ell} \left[ \frac{\cos(\varphi)}{(x - \frac{\ell}{2})^2 + y^2} - \frac{2[(\frac{\ell}{2} - x)\cos(\varphi) - y \sin(\varphi)](\frac{\ell}{2} - x)}{[(x - \frac{\ell}{2})^2 + y^2]^2} - \frac{\cos(\varphi)}{(x + \frac{\ell}{2})^2 + y^2} + \frac{2[(\frac{\ell}{2} + x)\cos(\varphi) + y \sin(\varphi)](\frac{\ell}{2} + x)}{[(\frac{\ell}{2} + x)^2 + y^2]^2} \right]. \tag{E1}$$

There are two limits of interest to be considered, namely the *dilute* limit corresponding to small inverse vortex temperatures $|\beta| \ll 1$ and the *dense* limit corresponding to large(-magnitude) inverse vortex temperatures, i.e. pairs of opposite-sign vortices for $\beta > 0$ and clusters of same-sign vortices for $\beta < 0$.

### 1. The dilute limit

In this case, the tails of the PDF of $\gamma$ are generated by events in which the perturbation is closer to a single point vortex than to any other vortices, i.e. $\mathbf{x}_p = \mathbf{x}_1 +$

$r(\cos(\phi), \sin(\phi))$, $r \ll \ell$. In this case,

$$\gamma \sim \frac{\Gamma_1\Gamma_2}{\ell r^2}\left[\sin(\varphi)\sin(2\theta) - \cos(\varphi)\cos(2\theta)\right] = -\frac{\Gamma_1\Gamma_2}{\ell r^2}\cos(2\theta+\varphi). \tag{E2}$$

Since we consider the case where $\varphi$ is optimal at every position, one finds $\varphi = -2\theta + n\pi$, $n \in \mathbb{N}$ and

$$\gamma \sim \frac{|\Gamma_1\Gamma_2|}{\ell r^2} \quad \Leftrightarrow \quad r(\gamma) \sim \sqrt{\frac{\gamma\ell}{|\Gamma_1\Gamma_2|}} \tag{E3}$$

Assuming that all ergophage positions are equally probable, then the probability of of being at distance betwenn $r$ and $r + dr$ is proportional to the ring area $2\pi r dr$. This can be inverted using (E3) to obtain a prediction for the PDF of $\gamma$, namely

$$P(\gamma) = r(\gamma)\frac{dr(\gamma)}{d\gamma} \propto \frac{1}{\gamma^2} \tag{E4}$$

### 2. The dense limit

In this case, the tails of the PDF of the growth rate stem from encounters of the localised perturbation with pairs of vortices, i.e. $\mathbf{x}_p = r(\cos(\theta), \sin(\theta))$, $r \gg \ell$. Then, one finds at leading order in $\ell$ that

$$\gamma \sim \frac{\Gamma_1\Gamma_2}{\ell}\left(-2\ell\frac{\cos(\varphi)\cos(\theta)}{r^3} + 2\ell\frac{y\sin(\varphi)(y^2-3x^2) - 2x\cos(\varphi)(x^2-x^2)}{r^6}\right) \sim -\frac{2\Gamma_1\Gamma_2}{r^3}\cos(3\theta-\varphi)$$

Again assuming that $\varphi$ is optimal, then $\varphi = -3\theta + n\pi$, $n \in \mathbb{N}$, such that

$$\gamma \sim \frac{2|\Gamma_1\Gamma_2|}{r^3},$$

which leads to the growth rate PDF, again under the assumption that all ergophage positions are equally probable

$$P(\gamma) = r(\gamma)\frac{dr(\gamma)}{d\gamma} \propto \frac{1}{\gamma^{\frac{1}{3}+\frac{4}{3}}} = \frac{1}{\gamma^{5/3}},$$

with an exponent $-5/3$, whose magnitude is less than 2, hence there is neither a finite mean nor a finite variance for this distribution. However, this $-5/3$ bears no relation to Kolmogorov's spectral exponent, it is merely a direct consequence of the modelling choices made here.


[1] A. van Kan, A. Alexakis, and M. E. Brachet, Extreme on-off intermittency, In preparation (2020).
[2] H. v. Helmholtz, LXIII. On integrals of the hydrodynamical equations, which express vortex-motion, The London, Edinburgh, and Dublin Philosophical Magazine and Journal of Science **33**, 485 (1867).
[3] G. Kirchhoff, *Vorlesungen über mathematische Physik: Mechanik*, Vol. 1 (BG Teubner, 1876).
[4] J. Goodman, T. Y. Hou, and J. Lowengrub, Convergence of the point vortex method for the 2-D Euler equations, Communications on Pure and Applied Mathematics **43**, 415 (1990).
[5] L. Onsager, Statistical hydrodynamics, Il Nuovo Cimento (1943-1954) **6**, 279 (1949).
[6] G. L. Eyink and K. R. Sreenivasan, Onsager and the theory of hydrodynamic turbulence, Reviews of Modern Physics **78**, 87 (2006).
[7] R. H. Kraichnan and D. Montgomery, Two-dimensional turbulence, Reports on Progress in Physics **43**, 547 (1980).
[8] P. Tabeling, Two-dimensional turbulence: a physicist approach, Physics Reports **362**, 1 (2002).
[9] G. Boffetta and R. E. Ecke, Two-dimensional turbulence, Annual Review of Fluid Mechanics **44**, 427 (2012).
[10] U. Frisch and A. N. Kolmogorov, *Turbulence: the legacy of AN Kolmogorov* (Cambridge University Press, 1995).
[11] A. Celani, S. Musacchio, and D. Vincenzi, Turbulence in more than two and less than three dimensions, Physical review letters **104**, 184506 (2010).
[12] H. Xia, D. Byrne, G. Falkovich, and M. Shats, Upscale energy transfer in thick turbulent fluid layers, Nature Physics **7**, 321 (2011).
[13] S. J. Benavides and A. Alexakis, Critical transitions in thin layer turbulence, Journal of Fluid Mechanics **822**, 364 (2017).
[14] A. van Kan and A. Alexakis, Condensates in thin-layer turbulence, Journal of Fluid Mechanics **864**, 490 (2019).
[15] S. Musacchio and G. Boffetta, Condensate in quasi-two-dimensional turbulence, Physical Review Fluids **4**, 022602 (2019).
[16] L. M. Smith, J. R. Chasnov, and F. Waleffe, Crossover from two-to three-dimensional turbulence, Physical review letters **77**, 2467 (1996).
[17] E. Deusebio, G. Boffetta, E. Lindborg, and S. Musacchio, Dimensional transition in rotating turbulence, Physical Review E **90**, 023005 (2014).
[18] A. Alexakis and L. Biferale, Cascades and transitions in turbulent flows, Physics Reports **767**, 1 (2018).
[19] E. D. Siggia and H. Aref, Point-vortex simulation of the inverse energy cascade in two-dimensional turbulence, The Physics of Fluids **24**, 171 (1981).
[20] G. Carnevale, J. McWilliams, Y. Pomeau, J. Weiss, and W. Young, Evolution of vortex statistics in two-dimensional turbulence, Physical review letters **66**, 2735 (1991).
[21] R. Benzi, M. Colella, M. Briscolini, and P. Santangelo, A simple point vortex model for two-dimensional decaying turbulence, Physics of Fluids A: Fluid Dynamics **4**, 1036

(1992).
[22] J. B. Weiss and J. C. McWilliams, Temporal scaling behavior of decaying two-dimensional turbulence, Physics of Fluids A: Fluid Dynamics **5**, 608 (1993).
[23] E. Trizac, A coalescence model for freely decaying two-dimensional turbulence, EPL (Europhysics Letters) **43**, 671 (1998).
[24] J. B. Weiss, Punctuated hamiltonian models of structured turbulence, Semi-Analytic Methods for the Navier–Stokes Equations (Montreal, Canada, 1995)(ed. K. Coughlin). CRM Proc. Lecture Notes **20**, 109 (1999).
[25] H. Aref, Stirring by chaotic advection, Journal of fluid mechanics **143**, 1 (1984).
[26] M. P. Rast and J.-F. Pinton, Point-vortex model for lagrangian intermittency in turbulence, Physical Review E **79**, 046314 (2009).
[27] M. P. Rast and J.-F. Pinton, Pair dispersion in turbulence: the subdominant role of scaling, Physical review letters **107**, 214501 (2011).
[28] M. P. Rast, J.-F. Pinton, and P. D. Mininni, Turbulent transport with intermittency: Expectation of a scalar concentration, Physical Review E **93**, 043120 (2016).
[29] B. Gallet and R. Ferrari, The vortex gas scaling regime of baroclinic turbulence, Proceedings of the National Academy of Sciences **117**, 4491 (2020).
[30] L. Horace, *Hydrodynamics*, 6th ed. (Dover, New York, 1945).
[31] H. Aref and E. D. Siggia, Evolution and breakdown of a vortex street in two dimensions, Journal of Fluid Mechanics **109**, 435 (1981).
[32] R. Krasny, A study of singularity formation in a vortex sheet by the point-vortex approximation, Journal of Fluid Mechanics **167**, 65 (1986).
[33] R. Krasny, Desingularization of periodic vortex sheet roll-up, Journal of Computational Physics **65**, 292 (1986).
[34] B. Nowak, J. Schole, D. Sexty, and T. Gasenzer, Nonthermal fixed points, vortex statistics, and superfluid turbulence in an ultracold bose gas, Physical Review A **85**, 043627 (2012).
[35] M. T. Reeves, T. P. Billam, B. P. Anderson, and A. S. Bradley, Inverse energy cascade in forced two-dimensional quantum turbulence, Physical review letters **110**, 104501 (2013).
[36] T. P. Billam, M. T. Reeves, B. P. Anderson, and A. S. Bradley, Onsager-kraichnan condensation in decaying two-dimensional quantum turbulence, Physical review letters **112**, 145301 (2014).
[37] A. Griffin, V. Shukla, M.-E. Brachet, and S. Nazarenko, Magnus-force model for active particles trapped on superfluid vortices, Physical Review A **101**, 053601 (2020).
[38] G. Joyce and D. Montgomery, Negative temperature states for the two-dimensional guiding-centre plasma, Journal of Plasma Physics **10**, 107 (1973).
[39] P.-H. Chavanis, J. Sommeria, and R. Robert, Statistical mechanics of two-dimensional vortices and collisionless stellar systems, The Astrophysical Journal **471**, 385 (1996).
[40] B. Gallet, Exact two-dimensionalization of rapidly rotating large-reynolds-number flows, Journal of Fluid Mechanics **783**, 412 (2015).
[41] B. Gallet and C. R. Doering, Exact two-dimensionalization of low-magnetic-reynolds-number flows subject to a strong magnetic field, Journal of Fluid Mechanics **773**, 154 (2015).
[42] K. Seshasayanan and B. Gallet, Onset of three-dimensionality in rapidly rotating turbulent flows, Journal of Fluid Mechanics **901**, R5 (2020).
[43] E. M. Purcell and R. V. Pound, A nuclear spin system at negative temperature, Physical Review **81**, 279 (1951).
[44] A. Oja and O. Lounasmaa, Nuclear magnetic ordering in simple metals at positive and negative nanokelvin temperatures, Reviews of Modern Physics **69**, 1 (1997).
[45] P. Medley, D. M. Weld, H. Miyake, D. E. Pritchard, and W. Ketterle, Spin gradient demagnetization cooling of ultracold atoms, Physical review letters **106**, 195301 (2011).
[46] X. Yu, T. P. Billam, J. Nian, M. T. Reeves, and A. S. Bradley, Theory of the vortex-clustering transition in a confined two-dimensional quantum fluid, Physical Review A **94**, 023602 (2016).
[47] F. Cornu and B. Jancovici, On the two-dimensional coulomb gas, Journal of statistical physics **49**, 33 (1987).
[48] G. Krstulovic, C. Cartes, M. Brachet, and E. Tirapegui, Generation and characterization of absolute equilibrium of compressible flows, International Journal of Bifurcation and Chaos **19**, 3445 (2009).
[49] J. B. Weiss and J. C. McWilliams, Nonergodicity of point vortices, Physics of Fluids A: Fluid Dynamics **3**, 835 (1991).
[50] A. A. Dubkov, B. Spagnolo, and V. V. Uchaikin, Lévy flight superdiffusion: an introduction, International Journal of Bifurcation and Chaos **18**, 2649 (2008).
[51] M. F. Shlesinger, G. M. Zaslavsky, and U. Frisch, *Lévy flights and related topics in physics* (Springer, 1995).
[52] A. V. Chechkin, R. Metzler, J. Klafter, V. Y. Gonchar, *et al.*, Introduction to the theory of lévy flights, Anomalous Transport , 129 (2008).
[53] B. B. Mandelbrot, *The fractal geometry of nature*, Vol. 173 (WH freeman New York, 1983).
[54] M. Shlesinger, B. West, and J. Klafter, Lévy dynamics of enhanced diffusion: Application to turbulence, Physical Review Letters **58**, 1100 (1987).
[55] T. Solomon, E. R. Weeks, and H. L. Swinney, Observation of anomalous diffusion and lévy flights in a two-dimensional rotating flow, Physical Review Letters **71**, 3975 (1993).
[56] R. Metzler and J. Klafter, The random walk's guide to anomalous diffusion: a fractional dynamics approach, Physics reports **339**, 1 (2000).
[57] B. Dubrulle and J.-P. Laval, Truncated lévy laws and 2d turbulence, The European Physical Journal B-Condensed Matter and Complex Systems **4**, 143 (1998).
[58] D. del Castillo-Negrete, B. Carreras, and V. Lynch, Nondiffusive transport in plasma turbulence: a fractional diffusion approach, Physical review letters **94**, 065003 (2005).
[59] C. Schinckus, How physicists made stable lévy processes physically plausible, Brazilian Journal of Physics **43**, 281 (2013).
[60] P. D. Ditlevsen, Anomalous jumping in a double-well potential, Physical Review E **60**, 172 (1999).
[61] P. D. Ditlevsen, Observation of $\alpha$-stable noise induced millennial climate changes from an ice-core record, Geophysical Research Letters **26**, 1441 (1999).
[62] I. Rhee, M. Shin, S. Hong, K. Lee, S. J. Kim, and S. Chong, On the levy-walk nature of human mobility, IEEE/ACM transactions on networking **19**, 630 (2011).

[63] B. Gross, Z. Zheng, S. Liu, X. Chen, A. Sela, J. Li, D. Li, and S. Havlin, Spatio-temporal propagation of covid-19 pandemics, medRxiv (2020).

[64] G. M. Viswanathan, V. Afanasyev, S. Buldyrev, E. Murphy, P. Prince, and H. E. Stanley, Lévy flight search patterns of wandering albatrosses, Nature **381**, 413 (1996).

[65] R. Metzler and J. Klafter, The restaurant at the end of the random walk: recent developments in the description of anomalous transport by fractional dynamics, Journal of Physics A: Mathematical and General **37**, R161 (2004).

[66] D. Applebaum, Lévy processes-from probability to finance and quantum groups, Notices of the AMS **51**, 1336 (2004).

[67] K. Kumar, S. Fauve, and O. Thual, Critical self-tuning: the example of zero prandtl number convection, Journal de Physique II **6**, 945 (1996).

[68] K. Kumar, P. Pal, and S. Fauve, Critical bursting, EPL (Europhysics Letters) **74**, 1020 (2006).

[69] N. Platt, E. Spiegel, and C. Tresser, On-off intermittency: A mechanism for bursting, Physical Review Letters **70**, 279 (1993).

[70] S. Aumaître, K. Mallick, and F. Pétrélis, Noise-induced bifurcations, multiscaling and on–off intermittency, Journal of Statistical Mechanics: Theory and Experiment **2007**, P07016 (2007).

[71] S. Benavides, E. Deal, J. Perron, J. Venditti, Q. Zhang, and K. Kamrin, *Multiplicative noise and intermittency in bedload sediment transport* (2020).

[72] M. Ding and W. Yang, Distribution of the first return time in fractional brownian motion and its application to the study of on-off intermittency, Physical Review E **52**, 207 (1995).

[73] A. Alexakis and F. Pétrélis, Planar bifurcation subject to multiplicative noise: Role of symmetry, Physical Review E **80**, 041134 (2009).

[74] A. Alexakis and F. Pétrélis, Critical exponents in zero dimensions, Journal of Statistical Physics **149**, 738 (2012).

[75] F. Pétrélis and A. Alexakis, Anomalous exponents at the onset of an instability, Physical Review Letters **108**, 014501 (2012).

[76] R. N. Mantegna and H. E. Stanley, Stochastic process with ultraslow convergence to a gaussian: the truncated lévy flight, Physical Review Letters **73**, 2946 (1994).

[77] A. van Kan, T. Nemoto, and A. Alexakis, Rare transitions to thin-layer turbulent condensates, Journal of Fluid Mechanics **878**, 356 (2019).